TRANSPORT WINDOW OF HIGH CURRENT HEAVY ION BEAMS IN A FINAL BUNCHER

Takashi Kikuchi, Mitsuo Nakajima and Kazuhiko Horioka

Department of Energy Sciences, Tokyo Institute of Technology, Nagatsuta 4259, Midori-ku, Yokohama, 226-8502, Japan

ABSTRACT

A longitudinal compression is indispensable in a final stage of the driver system for heavy ion inertial fusion. For the beam compression, an induction buncher applies the bunching voltage so as to make a considerable velocity tilt between the head and the tail of the beam bunch. At the first step of the design works for the beam transport line, the initial phase advance is decided to avoid resonance lines on the tune diagram. However, as the phase advance changes by the head-to-tail velocity tilt and the perveance increases during the beam bunching, the beam bunch sometimes reenters into the resonance condition. We estimate the dynamics of the bunching beams using a particle-core model. The stable transport region is discussed using a phase diagram. The transport window is illustrated in the diagram, as a function of the phase advance and the velocity tilt.

I. Introduction

In the field of heavy ion inertial fusion (HIF), an intense-heavy-ion beam is required for a suitable implosion of a fuel pellet.[1-3] In contrast to conventional particle accelerators, the required heavy ion beam has extreme parameters; the particle energy of ~10 GeV, the total beam current of ~100 kA and the pulse duration of ~10 ns. A longitudinal compression is indispensable in the final stage of the heavy-ion driver. In the region, the beam pulse duration must be compressed from ~100 ns to ~10 ns for the effective pellet implosion. For the beam compression, an induction buncher applies the bunching voltage so as to make a considerable velocity tilt between the head and the tail of the beam bunch.[4] Figure 1 shows one unit of the induction buncher system and the schematic of the beam bunching. The induction buncher

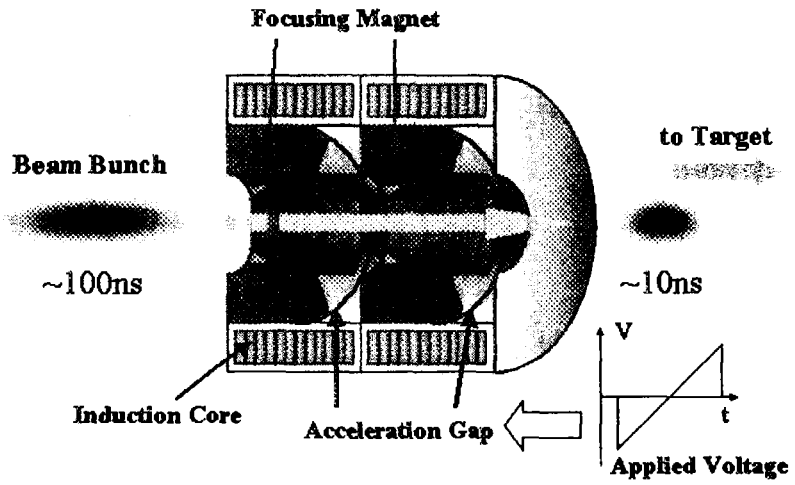

Fig.1: Induction buncher system and schematic of beam bunching.

unit consists of acceleration gaps and a focus-drift-defocus-drift (FODO) configuration lattice. At the first stage of design works for the beam transport line, the initial phase advance is decided to avoid resonance lines on the tune diagram. However, as the phase advance changes by the head-to-tail velocity tilt and the perveance increases during the beam bunching, the beam bunch reenters into resonance conditions. The transverse mismatch induced by those effects may cause a chaotic behavior, a halo formation and an emittance growth of the beam, during the compression process.

In this study, we estimate the dynamics and transport window of the bunching beams using a particle-core model (PCM).[5-7] The stable transport region is discussed on a phase diagram including a consideration about the envelope resonance of the mismatched beam. The transport window is illustrated in the diagram, as a function of the phase advance and the velocity tilt. Finally, we investigate the stability of particles during the bunching process using PCM calculations.

II. Descriptions of Beam Dynamics as Transverse and Longitudinal Envelope

We use beam envelope equations and PCM for the analyses of the bunching beam behavior. In this section, the longitudinal and transverse envelope equations are shown.[8] The transverse envelope dynamics X, Y along transport direction s are calculated by

$$\frac{d^2X}{ds^2} = -\tilde{k}_x X + \frac{2\tilde{K}}{X+Y} + \frac{\varepsilon_x^2}{X^3}, \tag{1a}$$

$$\frac{d^2Y}{ds^2} = -\tilde{k}_y Y + \frac{2\tilde{K}}{X+Y} + \frac{\varepsilon_y^2}{Y^3}, \tag{1b}$$

where ε_x, ε_y are the transverse emittances for the each direction. The K is the transverse modulated perveance expressed by,

$$\tilde{K} = \frac{q^2 N}{4\pi\varepsilon_0 mc^2 \tilde{\beta}^2 \tilde{\gamma}^3} \frac{1}{Z}, \tag{2}$$

where q is the charge of the beam ion, N is the number of the beam ion, ε_0 is the permittivity of free space, m is the mass of the beam ion, c is the speed of light, Z is the longitudinal beam envelope, β is the velocity divided by c and γ is the relativistic factor at the longitudinal beam position, respectively. The $\tilde{}$ indicates the modulated value due to the velocity tilt for the beam bunching. Here, the transverse confinement forces

$$\begin{aligned} \tilde{k}_x &= \tilde{k}h \\ \tilde{k}_y &= -\tilde{k}h \end{aligned}, \tag{3}$$

contain the periodical function h, in the case of FODO lattice which is given by

$$h = \begin{cases} 1 & (0 \le s \le \pi/2) \\ 0 & (\pi/2 < s \le \pi) \\ -1 & (\pi < s \le 3\pi/2) \\ 0 & (3\pi/2 < s \le 2\pi) \end{cases}, \tag{4}$$

and the transverse focusing parameter modulated by the velocity tilt is estimated as:

$$\tilde{k} = \frac{qB}{mc\tilde{\beta}\tilde{\gamma}a_q}, \tag{5}$$

where B is the magnetic force of the FODO lattice, a_q is the inner radius of the FODO magnet coil. Assuming the parabolic line charge density for the longitudinal direction as shown in

Table.1: Parameters for the calculations

Ion Species	Pb^{+1} (207.2 u)
Ion Number	2.5×10^{15}
Total Charge	0.4 mC
Pulse Duration	250 ns ⇒ 10 ns
Total Beam Current	1.6 kA ⇒ 40 kA
Beam Number	4
Current per Beam	400 A ⇒ 10 kA
Particle Energy	10 GeV (β~0.31)
Longitudinal Beam Length	23 m ⇒ 0.9 m
Initial Phase Advance	60 deg
Lattice Period	3 m

Fig.2, the longitudinal beam behavior can be described as:

$$\frac{d^2Z}{ds^2} = -k_z + \frac{K_L}{Z^2}. \tag{6}$$

Here k_z is the applied linear force for the beam bunching, K_L is the longitudinal perveance, which is defined by

$$K_L = \frac{3}{2}\frac{gNr_c}{\beta^2\gamma^5}, \tag{7}$$

g is the geometry factor and r_c is the classical particle radius. By numerically solving the above equations simultaneously, we can calculate the beam envelope dynamics.

Typical calculation results are shown in Figs.3 and 4. The longitudinal beam bunch behaviors are shown in Fig.3. Figure 4 shows the behavior of the transverse envelope along the transport direction at center (a) and at head (b) of the beam bunch. In this case, we use the parameters of Table.1 for the calculation. As shown in Fig.3, the beam bunch length is gradually shortened with the increase of the applied velocity tilt. In Fig.4(a), it is found that the envelope of the beam center is slightly spread due to the perveance increase. However, the envelope of the beam head shows the mismatched oscillation, because of the large head-to-tail velocity tilt, as shown in Fig.4(b). The mismatch oscillation of the beam envelope may induce

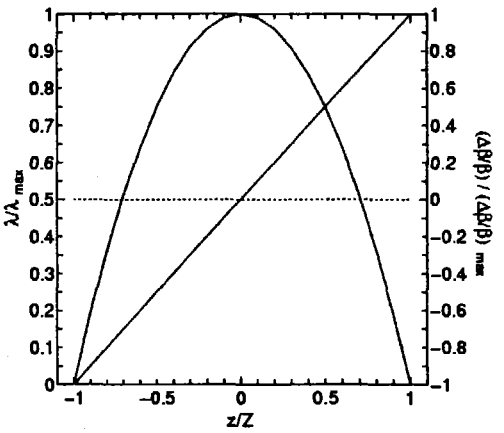

Fig.2: Distributions of longitudinal line charge density and velocity tilt ratio for bunching beam. The above values are normalized by maximum values.

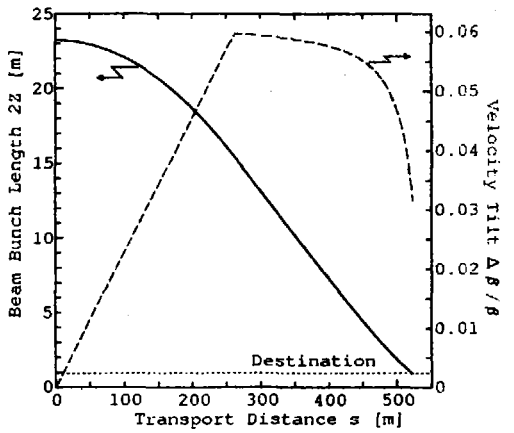

Fig.3: Longitudinal bunch length and velocity tilt during beam compression.

the irreversible emittance growth and the halo formation.[5-7)]

III. Transport Window and Results of PCM Calculation

In this section, we discuss a stably transportable region of the bunching beam on the phase space. It is well known that if the betatron tune of the beam enters to the forbidden values, the beam becomes resonantly unstable.[8)] The phase advance of 60deg is typical value of the resonance conditions. Usually, the initial phase advance (without space charge) σ_0 is depressed by the space charge effect. From this, the space charge depressed phase advance σ is automatically avoided from the resonance line even if the σ_0 is set at the resonance value. However, bunching beams with large compression ratio have inevitably large velocity tilts, and the phase advance is considerably modulated by the velocity tilt. The relations of the FODO lattice parameters and the phase advance are given as;

$$\tilde{k} = \frac{\beta\gamma}{\tilde{\beta}\tilde{\gamma}} k, \tag{8}$$

$$\cos\sigma_0 = \cos\theta\cosh\theta + \frac{L}{\ell}\theta(\cos\theta\sinh\theta - \sin\theta\cosh\theta) - \frac{1}{2}\left(\frac{L}{\ell}\right)^2\theta^2\sin\theta\sinh\theta, \tag{9}$$

$$k = \left(\frac{\theta}{\ell}\right)^2, \tag{10}$$

where ℓ is the length of the focusing space (F or D in FODO), L is the length of the drift space (O in FODO) and θ is the focusing strength of the magnetic lens.

The modulated phase advance by the velocity tilt is shown in Fig.5. Figure 5(a) shows the modulated phase advance as functions of the velocity tilt, at the head and the tail of the bunching beam. As Fig.5(a) shows, the phase advance at the beam head is increased with the velocity tilt. As mentioned previously, the phase advance is depressed by the space charge due to the velocity tilt, and the phase advance increased may cause the resonance reentrance. Consequently, the stable transport region is restricted by the resonance reentrance condition as a function of the velocity tilt. Figure 5(b) shows the transport window derived in this study. As expected, the beam transport with the initial phase advance of 60deg tends to cause the beam instability. In contrast to the case of the σ_0=60deg, the beam is expected to be transported with stable condition in the case of σ_0=56deg and $\Delta\beta/\beta \leqq 0.1$.

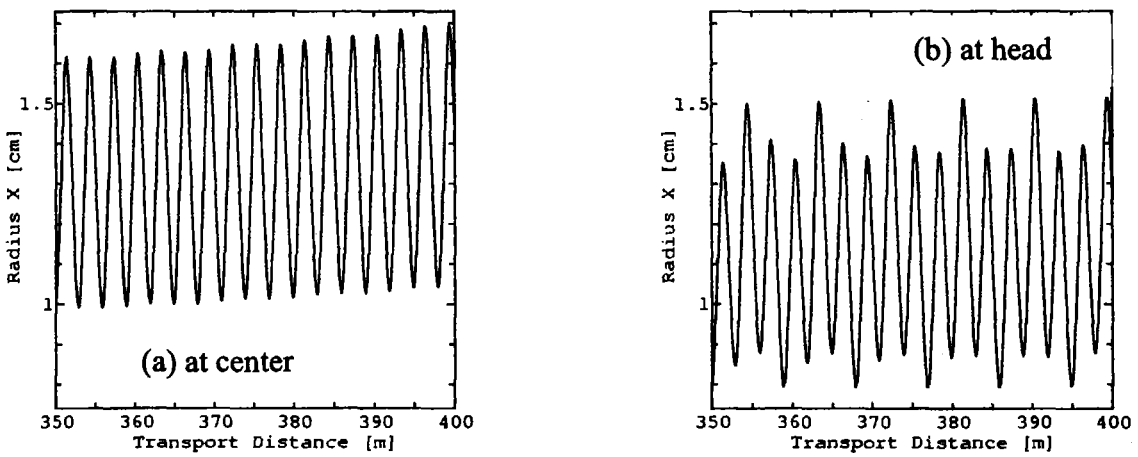

Fig.4: Typical results for transverse mismatch of bunching beam envelope. (a) shows beam envelope at the center, and (b) shows beam envelope at the head.

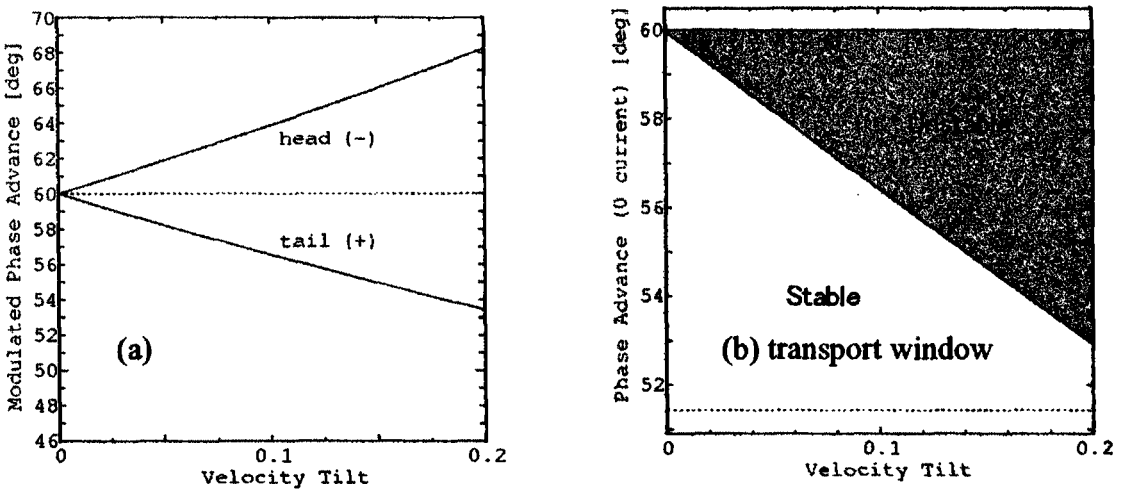

Fig.5: Expected phase advance modulated by velocity tilt (a) and transport window as a function velocity tilt (b).

Based on the above consideration, we carried out the PCM calculation. We investigate the stability of the beam particles on the phase space. For example, the test particle equations of x-direction are written by

$$\frac{d^2x}{ds^2} = -\tilde{k}_x x + \begin{cases} \dfrac{2\tilde{K}}{X(X+Y)}x & (|x| \le X) \\ \dfrac{\mathrm{sgn}(x)\cdot 2\tilde{K}}{|x| + \sqrt{x^2 + Y^2 - X^2}} & (|x| > X) \end{cases}, \tag{11}$$

where x is the position of a beam particle and

$$\mathrm{sgn}(x) = \begin{cases} +1 & (x > 0) \\ -1 & (x < 0) \end{cases}. \tag{12}$$

We can also calculate about y in the same manner, which is the position of a test particle along the y-direction. Using the above relations, we can investigate the particle evolutions of the bunching beam within the framework of PCM approximation. The beam instability is indicated by the scattering of test particles on the phase space. In this study, the perveance and

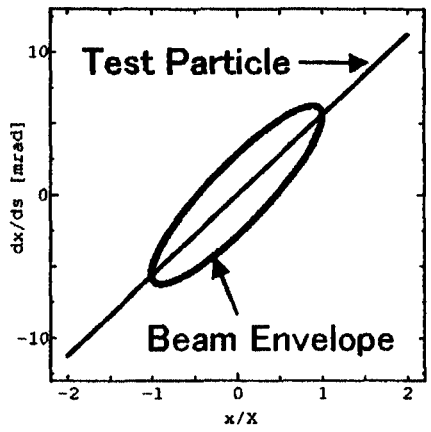

Fig.6: Initial distribution of beam envelope and test particles on phase space for x-direction.

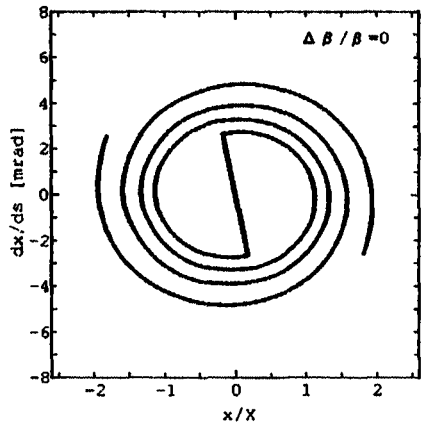

Fig.7: Typical example of test particle distribution on phase space in the case of matching beam after 150 lattice periods.

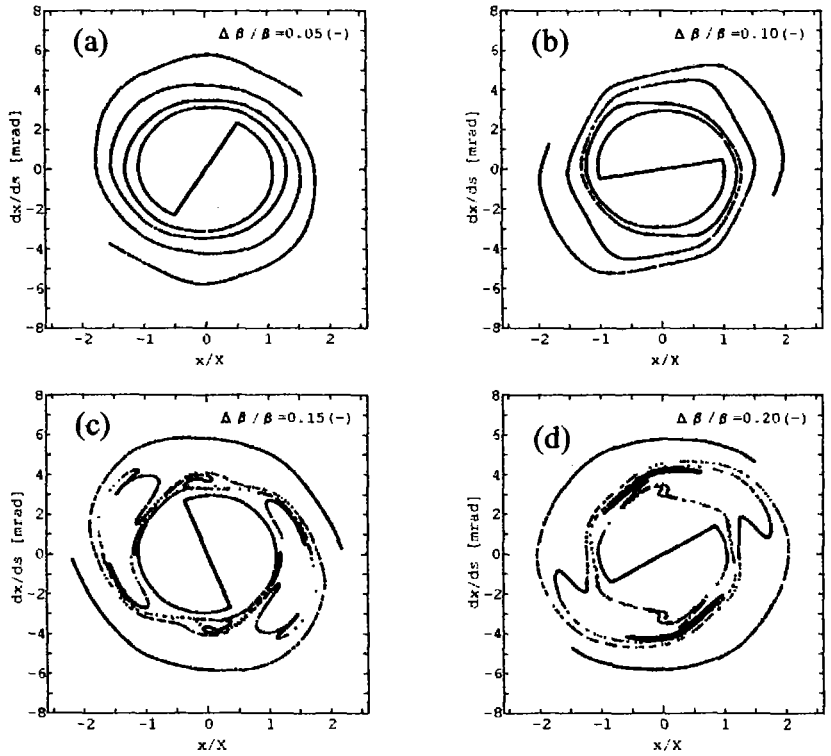

Fig.8: PCM calculation results after 150 lattice periods in the case of σ_0=60deg at the beam head. $\Delta\beta/\beta$ are (a) at 0.05, (b) at 0.10, (c) at 0.15 and (d) at 0.20, respectively.

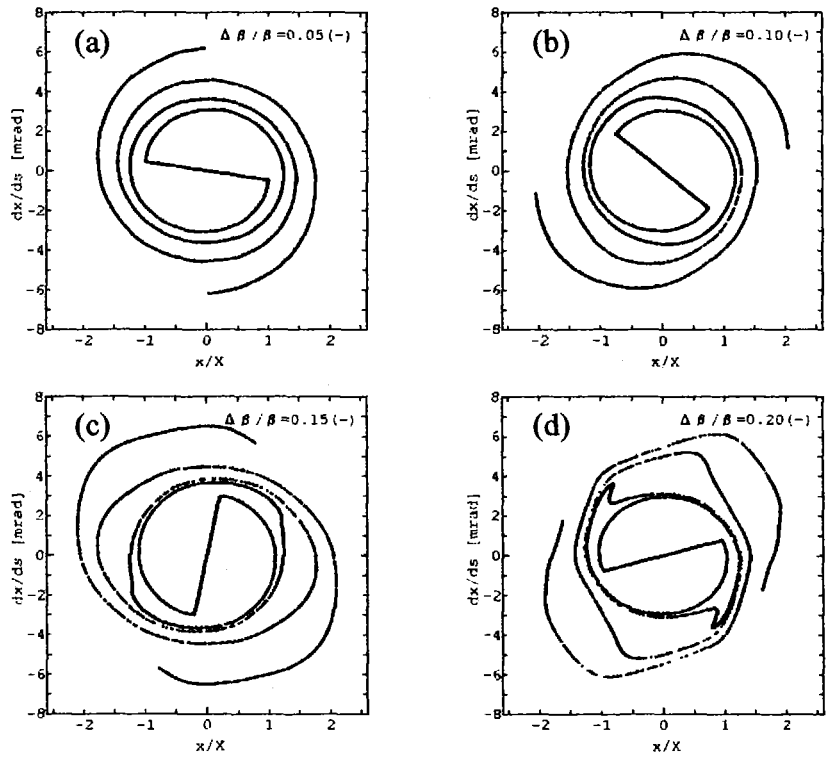

Fig.9: PCM calculation results after 150 lattice periods in the case of σ_0=56deg at the beam head. $\Delta\beta/\beta$ are (a) at 0.05, (b) at 0.10, (c) at 0.15 and (d) at 0.20, respectively.

the velocity tilt are assumed as constant during the beam transport for the clarification of the velocity tilt effect. Figure 6 shows the initial test particle distribution and beam envelope on the x-x' phase space. In the case of matched beam, the test particles are periodically evolved on the phase space as shown in Fig.7. However, as mentioned earlier, the velocity tilt causes the resonance reentrance, and the interaction between the resonance effect and the envelope mismatch due to the large velocity tilt induces the irregularity of the particle behaviors as shown in Fig.8. On the other hand, the bunching beam with σ_0=56deg can be stably transported as Fig.9 shows, in contrast to the case of σ_0=60deg. Although, detailed behaviors of the intense and highly bunched beam including the emittance growth must be investigated by more sophisticated models, these results indicate that the transport window as shown in Fig.8 can predict the bunching beam stability on the phase space.

IV. Conclusion

We investigated the transport window of the high current bunching beam using the beam envelope and PCM calculations. The stable transport region was estimated on the phase diagram, with a consideration about the envelope mismatch by the resonance. The transport window was illustrated in the diagram as a function of the phase advance and the velocity tilt. Using PCM calculations, we demonstrated the beam particle stability. As a result, it is found that those criterions can practically predict the transportability of the bunching beam. We believe that the criterion based on the transport window is useful as the first step evaluation of the transport line design for the final buncher in HIF.

References

1) J.J. Barnard, *et al.*, "Recirculating Induction Accelerators as Drivers for Heavy Ion Fusion", Phys. Fluids B, Vol.5 No.7, pp.2698-2706. (1993).
2) M. Reiser, "Physics of Intense Charged Particle Beams for Heavy Ion Inertial Fusion", Fusion Eng. Design, Vol.32-33, pp.133-140. (1996).
3) I. Hofmann, "Recent Developments in Heavy Ion Driver Studies at GSI", Proc. First Int. Conf. on Inertial Fusion Sci. and Applications, Bordeaux, pp.12-17. (1999).
4) M. Watanabe, M. Nakajima and K. Horioka, "Voltage Modulation and Repetitive Operation of Induction Ion Accelerator", Nucl. Instrum. Methods A464, pp.440-444. (2001).
5) J.-M. Lagniel, "Chaotic Behaviour and Halo Formation from 2D Space-Charge Dominated Beams", Nucl. Instrum. Methods A345 pp.405-410. (1994).
6) Q. Qian, R.C. Davidson and C. Chen, "Halo Formation Induced by Density Nonuniformities in Intense Ion Beams", Phys. Rev. E Vol.51 No.6 pp.5216-5219. (1995).
7) M. Ikegami, "Particle-Core Analysis of Mismatched Beams in a Periodic Focusing Channel", Phys. Rev. E Vol.59 No.2 pp.2330-2338. (1999).
8) M. Reiser, *Theory and Design of Charged Particle Beams*, Wiley, New York, (1994).

CHARACTERISTICS OF ENERGTIC IONS PRODUCED IN PLASMA FOCUS

M.Shiotani, K.Takao, T.Honda, I.Kitamura, T.Takahashi, and K.Masugata

Faculty of Engineering, Toyama University, 3190, Gofuku, Toyama, 930-8555, Japan

ABSTRACT

Characteristics of ion beams produced in the Mather type plasma focus (P.F) were studied experimentally to apply the beam to materials processing. The plasma focus was pre-filled with H_2 of 250 Pa, or mixture of H_2 (180 Pa) and N_2 (20 Pa). At 400 mm downstream from the top of the anode on the electrode axis, ion beam of current density ≈ 650 A/cm^2, pulse width ≈ 200 ns (FWHM) was observed when filling gas of H_2 was used. The ion species and energy spectra were evaluated by a Thomson parabola spectrometer (TPS). For protons of energy in the range of 0.1 - 1 MeV are observed when P.F was filled with H_2, where as protons and variety of nitrogen ions ($N^{(1-5)+}$) of energy in the range of 0.4 - 6 MeV are observed when using mixture gas. From the evaluation of the energy spectrum of nitrogen ions we see that the spectrum has a peak on 1 or 2 MeV. To evaluate the irradiation effect on materials, amorphous silicon films were irradiated by the ion beam and we see that amorphous silicon layers are crystallized by the irradiation.

Ⅰ. Introduction

Strong emission of energetic ions, electrons, and x-ray are known to be emitted from the pinch plasma produced in plasma focus (P.F.). Especially, the energetic ions have following characteristics and expected to be applied to materials processing. [1-5)]

a) High energy ions of energy ranging from 100 keV to several MeV are produced
b) Ion beam is obtained by relatively low voltage pulsed power systems.[6)]
c) The power density and the brightness of the beams are very high. [1)]
d) The ion species can be controlled by changing the filling gas.

To apply the ion beam to materials processing we have evaluated the characteristic of the ion beam. In addition, amorphous silicon films were irradiated by the ion beam to evaluate the irradiation effect on materials.

Ⅱ. Experimental apparatus

Figure 1 shows a schematic of the Mather type P.F. was used in the experiment. The P.F. consists of an anode, a rod cathode, and a glass insulator. The anode is a cylindrical copper electrode and the length and the diameter are 300 mm and 50 mm, respectively. To reduce the production of impurity ions and to reduce the damage of the electrode, the anode has a hollow shape top.

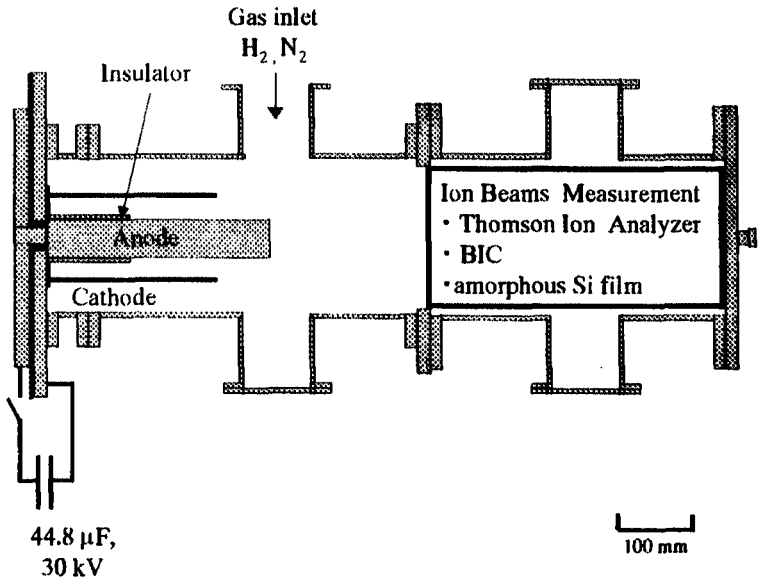

Fig. 1. Schematic of the experimental system.

The cathode consists of 24 copper rods of diameter 10 mm, length 230 mm and the effective inner diameter of the cathode is 100 mm. The insulator is made of glass and the length and the outer diameter are 125 mm and 55 mm, respectively.

To drive the P.F. a capacitor bank of capacitance 44.8 μF, maximum charging voltage 80 kV was used, which is connected to the P.F. through 28 of coaxial cables. In the experiment the charging voltage of the capacitor bank was fixed to 30 kV. The vacuum chamber was once evacuated to $< 7\text{x}10^{-3}$ Pa and after that filling gas was introduced. In the experiment pure hydrogen (250 Pa), and mixture gas of hydrogen (180 Pa) and nitrogen (20 Pa) were used as the filling gases.

To evaluate ion current density of the beam (J_i), biased ion collector (BIC) was used, which was placed in the gas filled vacuum chamber. The BIC has a cup electrode inside the grounded body and the ions are injected into the cup electrode through an aperture of diameter = 0.3 mm . The electrode was biased to -1 kV to remove commoving electrons.

For the measurement the species of ions and their energy spectra, Thomson parabola spectrometer (TPS) was used. The TPS is constructed of a first pinhole, a second pinhole, a magnetic deflector, an electrostatic deflector, and a ion track detecting film of CR-39, the detail of which is shown in the leterature[1].

Ⅲ. Experimental results

Figure 2 shows typical waveforms of the discharge current (I_d) measured by a Rogowski coil, and J_i measured at z = 400 mm downstream from the top of the anode on the electrodes axis. In the experiment the P.F. was pre-filled with pure hydrogen. As seen in the figure, I_d has a peak of 600 kA at t = 1.55 μs and after that 100 kA of current dip is observed, which suggest the strong pinch of the plasma. Ion current density rises sharply at t = 1.6 μs and a peak value of 650 A/cm^2 is observed with pulse width of 200 ns (FWHM).

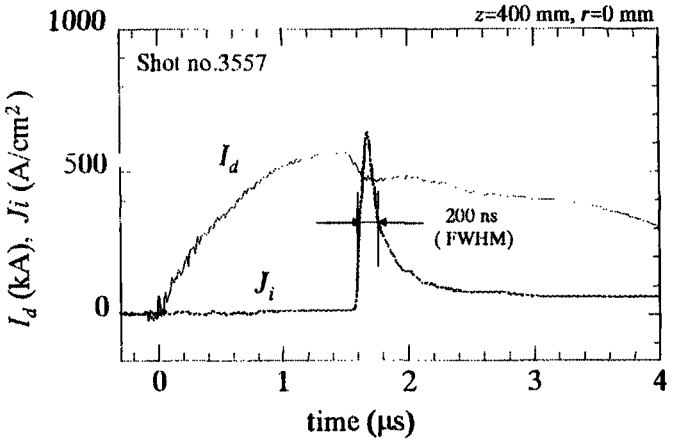

Fig. 2 Typical waveforms of I_d and J_i .

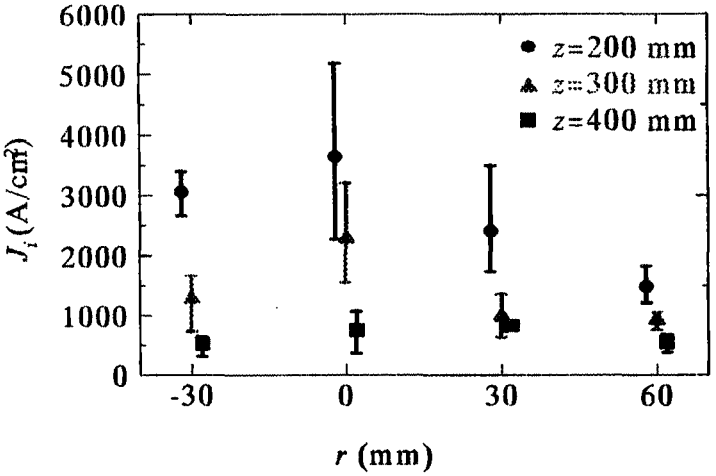

Fig. 3 Space distribution of J_i.

Figure 3 shows the distribution of the peak value of J_i obtained by BIC. As seen in the figure, at z = 200 mm, very large value of J_i = 3600 A/cm^2 is observed on the axis (r = 0).

Figure 4 shows the ion track pattern obtained by TPS. As seen in the figure, strong

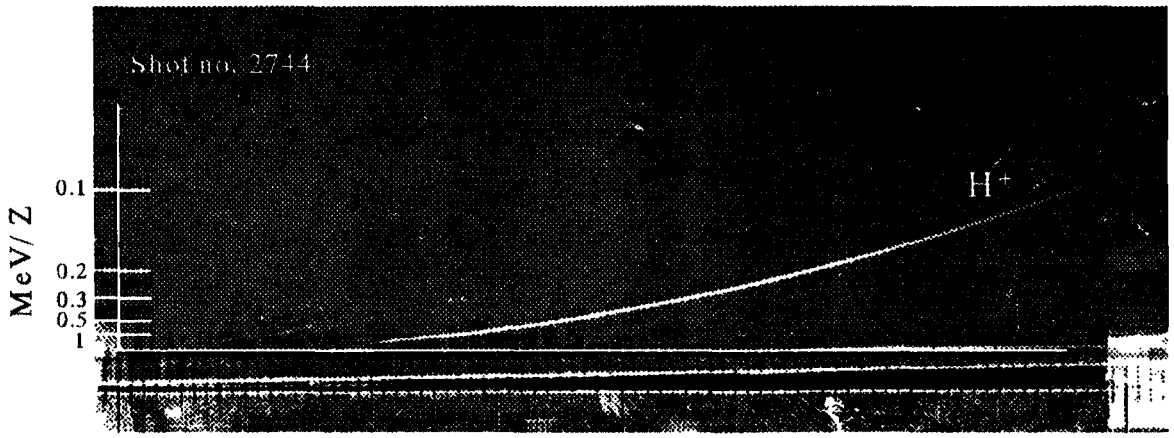

Fig. 4. The track pattern obtained by TPS. The filling gas was H_2 250 Pa.

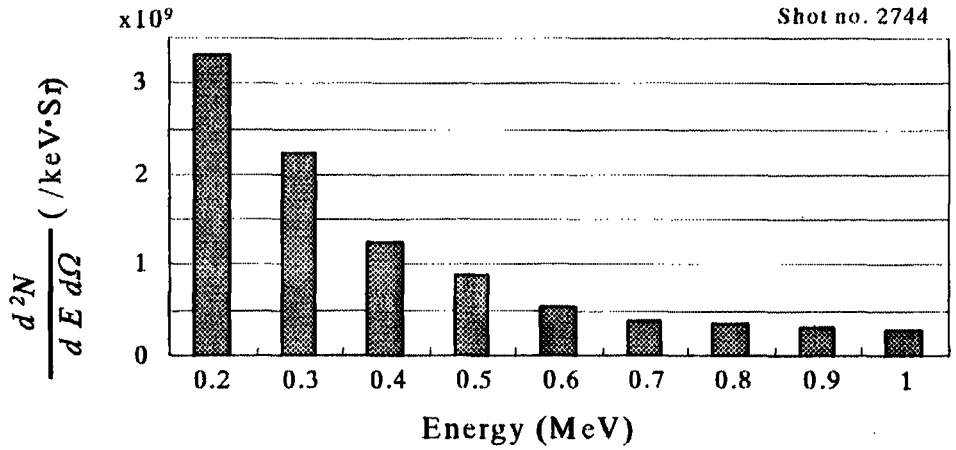

Fig. 5. Energy spectrum of protons evaluated from Fig. 4.

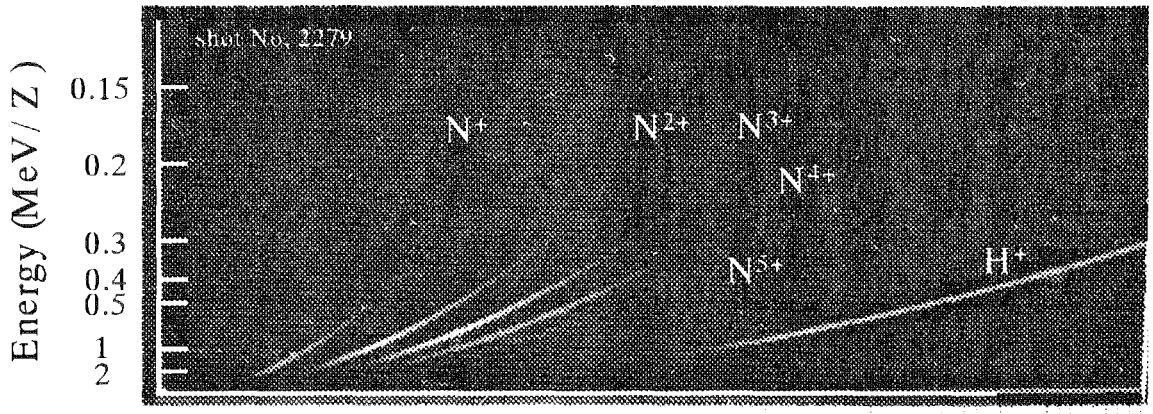

Fig. 6. The track pattern obtained with the TPS at mixture gas.

trace of protons is observed with weak trace of impurities. The energy of the protons is in the range of 0.1 - 1 MeV.

From the evaluation of ion track densities in Fig. 4, we have evaluated the energy spectrum of protons, which is shown in Fig. 5. From the figure, we see that proton flux decreases with increasing energy.

Figure 6 shows the track pattern obtained with TPS when mixture of H_2 and N_2 was used. As seen in the figure, variety of nitrogen ions ($N^{(1-5)+}$) are observed with protons. The energy of nitrogen ion is in the range of 0.4 - 6 MeV. In addition, no impurity ions was observed in the condition.

Figure 7 shows the energy spectra of nitrogen ions obtained from Fig. 6. As seen in the figure the each energy spectrum has a peak around 1 or 2 MeV. In addition we see that the average energy tend to be higher for highly ionized ions.

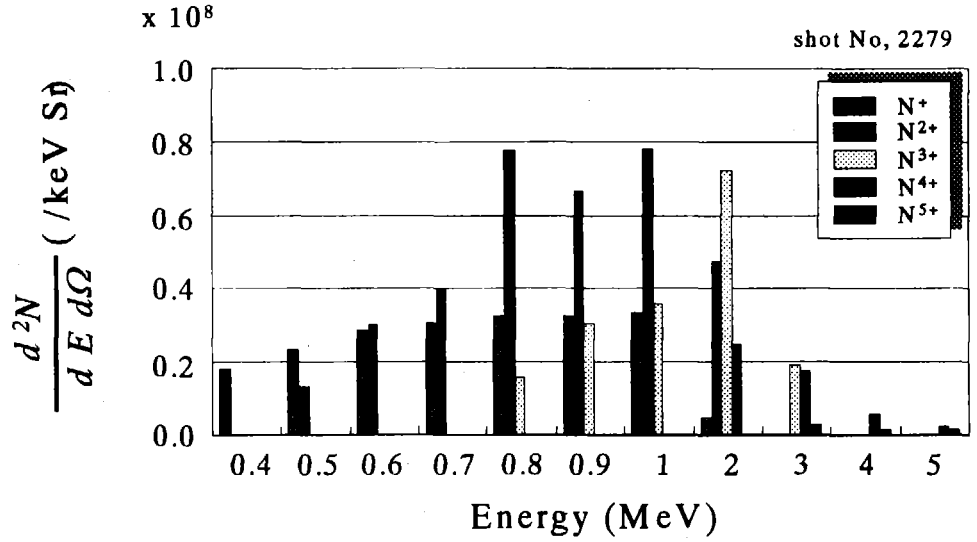

Fig. 7. Energy spectrum of nitrogen ion when mixture gas is used.

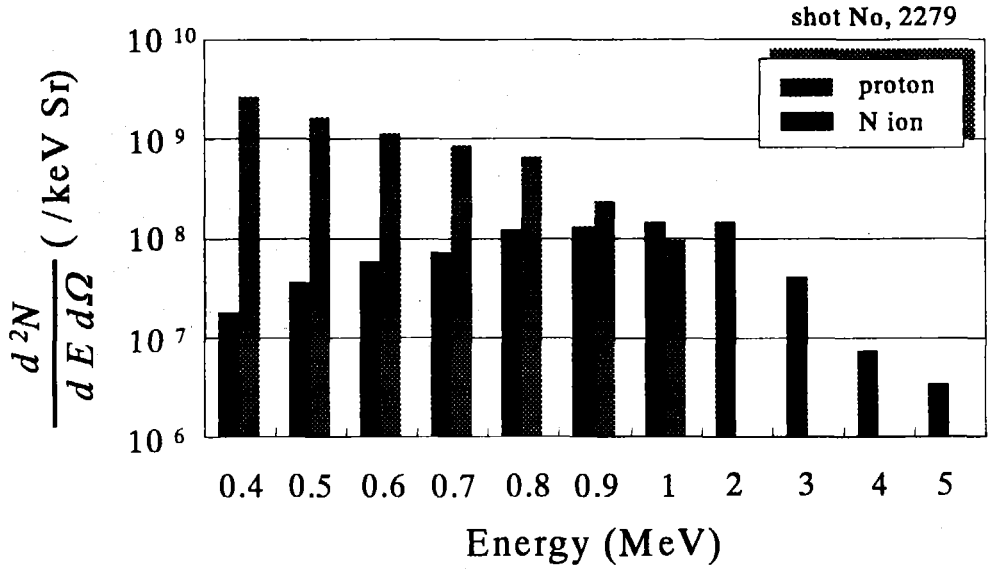

Fig. 8. Energy spectra of protons and nitrogen ions.

Figure 8 shows the energy spectrum of protons and nitrogen ions. As seen in the figure we found a clear difference between them. For protons the spectrum decrease monotonically with energy, whereas clear peak is observed in the spectrum of nitrogen.

IV. Irradiation Experiment

By the irradiation of intense pulsed ion beam to materials, the surface will pulse heated to extremely high temperature and the crystal structure is expected to be modified. To demonstrate the modification effect, amorphous silicon films were irradiated by the ion beam produced in P.F. The films were deposited on soda glass substrates by a vacuum evaporation technique. The size and the sickness of the targets are, 10 × 10 mm and 800 nm, respectively.

In the experimental P.F was operated on the same condition as that shown in Fig. 2-5 to irradiate proton beam. Figure 9 shows the positions of the targets in the experiment. The targes were placed at z = 400 mm and different radial positions. The ion current densities of each position can be estimated from Fig. 3.

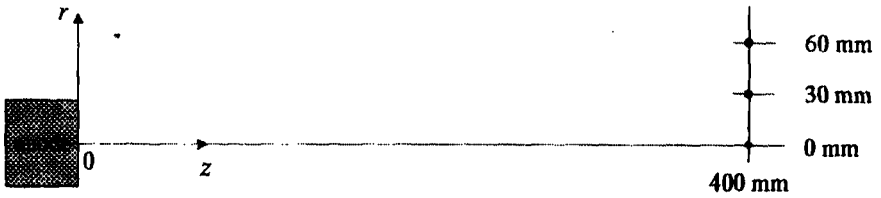

Fig. 9. The target positions in the irradiation experiment.

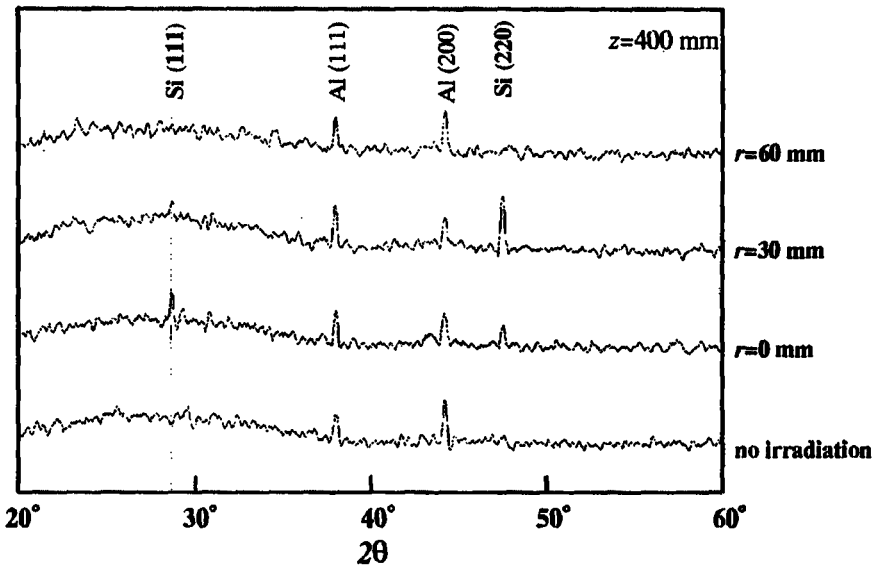

Fig. 10 X-ray diffraction patterns of amorphous Si thin films irradiated by pulsed proton beam.

Figure 10 shows the x-ray diffraction patterns of the films before and after one shot of beam irradiation. Here, the peaks correspond to Al are due to that Al holder is used in the diffraction measurement. From the figure we see that there is no crystal stricture in the target before irradiation. In contrast, in the diffraction patterns for the targets irradiated at r = 0 and 30 mm, we clearly see the peaks corresponding to Si (111) and Si (220), which indicate that amorphous silicon layer was crystallized by the irradiation of the beam. The target irradiated at r = 60 mm was not crystallized. This seems to be due to the insufficient beam intensity since it is much lower in that position.

Ⅳ. Conclusion

Characteristics of ion beams produced in the Mather type P.F were studied experimentally to apply the beam to materials processing. The P.F was pre-filled with H_2 of 250 Pa, or mixture of H_2 (180 Pa) and N_2 (20 Pa). At 400 mm downstream from the top of the anode on the electrode axis, ion beam of current density ≈ 650 A/cm^2, pulse width ≈ 200 ns

(FWHM) was observed when filling gas of H_2 was used. The ion species and energy spectra were evaluated by a Thomson parabola spectrometer (TPS). For protons of energy in the range of 0.1 - 1 MeV are observed when P.F was filled with H_2, where as protons and variety of nitrogen ions ($N^{(1-5)+}$) of energy in the range of 0.4 - 6 MeV are observed when using mixture gas. From the evaluation of the energy spectrum of nitrogen ions we see that the spectrum has a peak on 1 or 2 MeV. To evaluate the irradiation effect on materials, amorphous silicon films were irradiated by the ion beam and we see that amorphous silicon layers are crystallized by the irradiation.

References

1) K. Takao, Y. Doi, S. Hirata, M. Shiotani, I. Kitamura, T. Takahashi and K. Masugata, Jpn. J. Appl. Phys., **40**, Part 1 (2000) pp. 1013-1015

2) T. Takao, M. Shiotani, T. Honda, I. Kitamura, T. Takahashi, K. Masugata, Characteristics of the Nitrogen Ion Beam Produced in a Plasma Focus Device, Proc. 28th IEEE Int'l Conf. on Plasma Science and 13th IEEE Int'l Pulsed Power Conf., Las Vegas, Nevada, June 17-22, 2001, P1C01 (2001)

4) J. N. Feugeas, E. C. Llonch, C. O. de Gonzalez and G. Galambos, J. Appl. Phys., **64** (1988) 2648

5) H. Kelly, A. Lepone, A. Marquez, D. Lamas and C. Oviedo, Plasma Sources Sci. Technol. **5** (1996) 704

6) R.L. Gullickson and H.L. Sahlin, J. Appl. Phys., **49**, (1978) 1099